In: Magnetite: Structure, Properties and Applications ISBN: 978-1-61761-839-0
Editor: Dawn M. Angrove

Chapter 6

MAGNETITE: ELECTROCHEMICAL PROPERTIES AND ITS ROLE ON FLOW ACCELERATED CORROSION

Ki-Sok Jung[1] and Ki-Woung Sung[2*]

[1]Nuclear Fusion Engineering Development Division, Korea Atomic Energy Research Institute, 150 Dukjin-Dong, Yuseong-gu, Daejeon, 305-353, The Republic of Korea
[2]Nuclear Materials Research Division, Korea Atomic Energy Research Institute, 150 Dukjin-Dong, Yuseong-gu, Daejeon, 305-353, The Republic of Korea

ABSTRACT

Magnetite, an oxide of iron, is a semiconductor with a band gap of 0.1 eV which is quite low compared to those of other iron oxides or semiconductors. This results in a unique electrochemical property among similar materials. In an alkaline solution at ambient conditions, OH^- ions adsorb onto magnetite surfaces. It is found that at reducing polarization in an alkaline solution, two electrochemical signals, which come from the reduction of water molecules, appear on the magnetite electrode which can be related to the energy levels of magnetite.

In the power plant coolant circulating system where carbon steel is used for the feeding pipes, flow accelerated corrosion (FAC) results from the dissolution of normally protective magnetite film on piping materials. In order to investigate the dependency of FAC of carbon steel (A106 Gr. B) and low-alloy steels (1Cr-½Mo, 2¼Cr-1Mo), on pH, orifice distance and material, experiments were carried out. These were done under a flow velocity of 4 m/sec (partly 9 m/sec) at pH 8.0~10.0 in an oxygen-free aqueous solution re-circulated in an Erosion-Corrosion Test Loop at 130℃ for 500 hours. The weight loss of the carbon steel specimens appeared to be positively dependent on the flow velocity. Specimens of the carbon steel and low-alloy steels also showed to be distinguishably dependent on the pH. At 8.0~9.5 they decreased, but increased from 9.5 to 10.0. Utility water chemistry personnel should carefully consider this kind of pH dependency in order to control the pH of a water system for the mitigation of a FAC of the piping system material. The weight loss of the specimens located further from the orifice in the distance range of 6.8~27.2 mm was shown to be greater, except for 2¼Cr-

* Corresponding author: E-mail: ksjung@kaeri.re.kr, kisokj@gmail.com(JKS); kwsung@kaeri.re.kr(KWS)

1Mo that showed no orifice distance dependency. Low alloy steel specimens exhibited a factor of two times better resistance to FAC than that of the carbon steel. Based on this kind of dependency of FAC of the carbon and low-alloy steels on the orifice distance and material, it would be necessary to alternate the composition of the secondary piping system material of NPPs, with low-alloy steels such as 2¼Cr-1Mo, particularly when utility has to replace the system piping [1].

On the other hand, hydrazine concentration in the secondary water chemistry system has been maintained in the range of 100~150 ppb at the domestic nuclear power plants in Korea. But EdF in France showed that a hydrazine concentration in this range had an influence on the carbon steel flow-accelerated corrosion (FAC) at a temperature over 200℃, while Mitsubishi Heavy Industries in Japan and the British Energy in England did not. To improve the secondary water chemistry control, it is necessary to identify whether a carbon steel FAC is influenced by the hydrazine concentration or not. K. S. Sung et al. carried out an experiment on the effect of the hydrazine concentration on a carbon steel FAC at $pH_{25℃}$ of 9.0 controlled with ammonia in a deoxygenated aqueous solution re-circulated in a FAC test loop at 250℃ for 300 hours. The loop provided a flow velocity by a magnetically driven rotating blade onto the surface of the test specimens located outside of it, with a rotating speed of 1500 rpm. The relative specific weight loss obtained with hydrazine concentration of 0, 50, 100, 150 and 250 ppb was approximately 1.0, 1.14, 1.04, 0.63 and 0.70, respectively. These result showed the hydrazine concentration dependency of carbon steel FAC in this concentration range, appearing a maximum at the concentration of 50 ppb. This tendency is a little different from that of the EdF data. A continuous study is being carried out to re-evaluate the result [2].

Keywords: Carbon Steel, Cyclic Voltammetry, EIS, Flow-Accelerated Corrosion, Low-alloy steels, Magnetite, Polarization, Weight Loss

1. INTRODUCTION

Magnetite, Fe_3O_4, is one form of iron oxides like hematite (α-Fe_2O_3), maghemite (γ-Fe_2O_3), and wustite (FeO). Naturally magnetized pieces of magnetite, called lodestone, were used as magnetic compass needles in the great voyage era. In the power plant, irrespective of nuclear or fossil fuel powered, magnetite is formed as a corrosion product of carbon steel piping materials. Magnetite has an inverse spinel structure with cations in octahedral (o) and tetrahedral (t) sites. The unit cell has the formula $(Fe_8^{3+})_t[Fe_8^{3+}Fe_8^{2+}]_oO_{32}$ [3] in the fcc lattice of O^{2-} ions. Measurement of magnetite resistivity was made by Itai, et al [4]. They plated the ends of magnetite block with Cu and recorded the logarithmic value of resistivity (Ω-cm) to be -1.8.

Electrochemical properties of magnetite were mainly studies in relation to the flow assisted corrosion (FAC) of high temperature coolant piping in the power plant steam supply systems. There have been several electrochemical studies of magnetite electrodes [5, 6, 7]. Allen et al. [5] studied the capacitance and resistance of magnetite admixed with carbon in $NaClO_4$ solution at 22°C. Their conclusion was that the current flowing in the electrode is controlled by a solid-state diffusion process in which H^+ moves through the electrode. Allen et al. [6] worked on polycrystalline magnetite electrode in $NaClO_4$ solution and obtained different carrier concentrations at different potentials. They concluded that at high potentials the semiconductor properties of magnetite gave way to the properties of Fe_2O_3. Buchler et al.

[7] studied the passive films on iron in borated buffer solutions at pH 8.4. They concluded that Fe^{2+} was the doping species contributing to electronic properties, and the dopant concentration was dependent on potential changes. Bignold [8] studied the behavior of an iron electrode in a 1 M NaOH solution at 238 °C and obtained reduction peaks corresponding to $Fe_2O_3 \rightarrow Fe_3O_4$ at +0.336 V and +0.266 V with the corresponding oxidation peak at +0.596 V, all vs. SHE. Wielant et al. [9] studied the electronic properties of thermally-formed films of iron oxide and deduced semiconductor properties using the Mott–Schottky analysis. Their conclusion was that the doping concentration or charge carrier density N_D of air-formed oxide films was five times lower than the oxides formed in N_2, and that more negative flatband potentials were obtained for the oxides formed in N_2. Literature of magnetite pellet manufacturing and their utilization for electrochemical characterization is scarce and the results are discrepant.

Magnetite is the major corrosion product in both nuclear and fossil power plants [10, 11, 12]. Depending on the proportion of nickel alloys in the circuit, corrosion products in the primary heat transport system of a nuclear power plant (NPP) are a magnetite structure and contain a small amount of nickel [13]. In the secondary heat transport system, the major corrosion product is magnetite. The rapid thinning of carbon steel feeder pipes at the reactor outlet at some CANDU NPP was mainly due to FAC, which was caused by the removal of the normally protective magnetite film by coolant under-saturated in dissolved iron [12].

Since the major rupture at Trojan occurred in 1985, about 270 wall-thinning records have been reported for pressurized water reactors (PWRs) and about 115 records for boiling water reactors (BWRs) as of 1995, as shown in Figure 1 [14]. The inspections triggered by the failure that occurred at the Surry Unit 2 in 1986 have revealed numerous instances of significant erosion-corrosion at other U.S. reactors, primarily in wet-steam lines, but also in some single-phase lines. German data files for the period 1961 to 1976 showed that one-third of the 96 cases reported were for single-phase conditions [15]. A pipe rupture occurred as recently as 2004, as shown in Figure 2 [16].

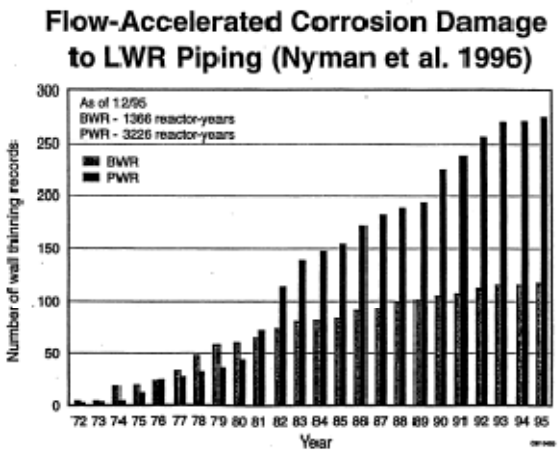

Figure 1. World-wide experience of the flow accelerated corrosion damage to LWR secondary-side piping [3]

Figure 2. A recent pipe rupture accident occurred at the position just after a flow-meter with an orifice-typed device, reported in 2004 [16]

Wall thinning is generally caused by flow accelerated corrosion (FAC) and leads to pipe rupture with no warning unless it is detected and repaired in a timely manner. A FAC is an acceleration or increase in the rate of the corrosion caused by the relative movement between a corrosive fluid and a metal surface. The root cause of the FAC process is the dissolution of the normally protective oxide layer from the metal surface, leading to a local thinning of the oxide and a subsequent increase in the corrosion rates resulting from a rapid diffusion through the oxide film [17]. Factors influencing a FAC include the flow velocity, steam quality, flow path geometry, water chemistry and pH, alloy content, and temperature [18-21].

A very important variable affecting a resistance against a FAC or erosion-corrosion of carbon and low alloy steels is the temperature. Most of the reported cases of FAC damage under single-phase conditions have occurred at 80~230℃. The highest rate of FAC under single-phase condition occurs at 130℃, particularly in an oxygen-free aqueous solution [15, 22-23].

On the other hand, a pH control is also one of the most important factors, and many experiments have been carried out showing the pH dependency of carbon steel FAC usually in a pH range up to about 9.5. The results show that the carbon steel FAC usually decreased with an increasing pH [14-24]. In order to confirm whether FAC would decrease even in the pH range over 9.5, and to confirm the influence of flow velocity, orifice distance and material, Sung et al. [1] investigated the dependencies of a single-phase FAC of carbon steel (A106 Grade B) and low-alloy steels (1Cr-½Mo and 2¼Cr-1Mo). The pH was controlled in the range from 8.0 to 10.0 with ammonia in an oxygen-free aqueous solution. The solution was re-circulated in an Erosion-Corrosion Test Loop under a flow velocity of 4 m/sec or 9 m/sec at 130℃ for 500 hours.

Furthermore, hydrazine concentration in the secondary water chemistry system at the domestic nuclear power plants in Korea has been maintained in the range of 100~150 ppb. Hydrazine, in the absence of the effect on oxygen, i.e., with a constant oxygen concentration, reduces the rate of a material loss, principally by increasing the system pH_T. However, if the hydrazine reduces the oxygen concentration to below the level required to inhibit a FAC, the effect of the reduction in the oxygen concentration can outweigh the benefit of the increase in pH, provided by the hydrazine. If this occurs, the net effect of an increase in hydrazine can be

an increase in a material loss occurring as the hydrazine is increased. A statistical evaluation of plant data for US PWRs in 1995 showed no correlation between low levels of oxygen and increased iron transport. However, since that time some plants have noted increased iron transport when oxygen levels are very low and, in response, are maintaining minimum condensate oxygen above a threshold value such as 2 to 3 ppb [25].

On the other hand, the effect of the hydrazine concentration on a FAC has been studied by EdF using a test loop [26, 27]. While there was a considerable scatter in the data, the main conclusions of this work were: (1) at a temperature of 235℃ (455℉), and with a near constant but a relatively low pH_T of 5.9~6.0, the FAC rates increased with an increasing hydrazine up to about 200 ppb, with the maximum increase being about a factor of 2, (2) for temperatures in the range of 180~195℃ (356~383℉), hydrazine did not appear to affect the FAC rate; however, this is contrary to earliest tests with the same loop, and it is thus uncertain, and was checked by additional tests. The most recent testing demonstrated that at 180℃, hydrazine had no measurable effect on a FAC, except to raise the pH. Additional studies are under way to re-evaluate the results at 235℃ and to address other parameters such as the pH, temperature, and transit time [25]. To evaluate the effect of the hydrazine concentration on a carbon steel FAC, K. W. Sung et al. also carried out an experiment at $pH_{25℃}$ of 9 controlled with ammonia in a deoxygenated solution in a FAC test loop at 250℃ for 300 hours [2].

2. MAGNETITE AS A SEMICONDUCTING MATERIAL

According to Cornell and Schwertmann [28], magnetite is both n- and p-type semiconductor, and its band gap is quite small (0.1 eV) compared to other iron oxides, e.g., 2.2 eV for hematite; 2.03 eV for maghemite; and 2.3 eV for wustite. Thus its conductivity 10^2-10^3 $\Omega^{-1}cm^{-1}$ is almost metallic because of the exchange of electrons between ferric and ferrous cations [29]. This low band gap is only four times of the room temperature energy (0.025V).

Meanwhile, Jung and L. de Pierrefeu [30] estimated the band gap of magnetite to be 0.14eV by the distance of two reduction peaks in the alkaline solution, which value corresponds to the infrared light energy. So it is supposed that magnetite can be a candidate material for the detection of infrared light. According to Dobson [3], the addition of zinc to the magnetite structure, expressed as $Zn_xFe_{3-X}O_4$, results in a variation of conductivity with x, suggesting that the system is metallic in type in the range $0 \leq x \leq 0.6$ and n-type semiconductor in the range $0.8 \leq x \leq 1.0$. As the resistivity of $Zn_xFe_{3-X}O_4$ increases exponentially when x nears the value one, it can be supposed that the addition of zinc in the coolant system with carbon steel pipes would strengthen resistivity against the FAC degradation. This is analogous to the zinc addition to the primary coolant circuit in the NPP for the suppression of crud formation and primary water stress corrosion cracking.

According to Jung and L. de Pierrefeu [30], electrolytic currents on the magnetite electrode in 0.1~0.5M LiOH solution increased each time cyclic voltammetric polarization was made, where the scan direction was from positive potential to negative, then reversed. This phenomenon was deemed very unique, and it was suggested that donor densities in magnetite increased each time cyclic voltammetric scan was performed. To verify this supposition, capacitance of the magnetite electrode – LiOH solution interface was measured

at different potentials and the resultant Mott-Schottky graph was obtained from the result. This experimental system apparently deviated from the ideal Randles behavior, and thus concept of constant phase elements (CPE) represented by the pseudo-capacitance (PC) should have been used for capacitance estimations [31]. According to Devilliers and Mahe [31], concepts of CPE and PC can be described by the following equation:

$$C_{SC} = \frac{1}{(2\pi \cdot f)^{p} \cdot Z_{imag}} \quad (1)$$

where C_{sc} is the capacitance of the space charge region of semiconductor, Z_{imag} is the capacitive component of impedance value, p is a non-dimensional coefficient which is obtained from the relation $\theta = (1-p)\frac{\pi}{2}$. The angle the plot makes with the vertical line is θ. This value was obtained when Jung and L. de Pierrefeu [30] plotted the impedance plane plot to the infinitely low frequency. Usually their experimental system showed $\theta = 15.8^{\circ}$, or p = 0.83. Then capacitance of the magnetite - electrolyte interface could be estimated, utilizing the Mott-Schottky relation below [32, 33]:

$$\frac{1}{C_{SC}^2} = \frac{2}{e\varepsilon\varepsilon_0 N_d}\left(-\Delta\phi - \frac{kT}{e}\right) \quad (2)$$

where C_{sc} is the capacitance of the space charge region, e is electronic charge, ε dielectric constant of magnetite, ε_0 is the vacuum permittivity, N_d is the donor density, k is Boltzmann constant, T is temperature in absolute scale, and $-\Delta\phi = E - E_{fb}$. Here is the electrode potential and E_{fb} is the flat band potential (FBP).

In the experiment of Jung and L. de Pierrefeu, ratios of donor concentrations before and after many cycles of CV were obtained by Eq. (2). After 17 cycles of CV, donor concentration increased 2.3~3.5 times than the one before CVs. This increase was attributed to the change like $Fe^{3+} \rightarrow Fe^{2+}$ in magnetite, and it was conceived that magnetite structure could be changed by this transition. This possibility seemed plausible when there were detections of black smudges detaching from the magnetite surface after more than ten cycles of CVs.

However, Jung and Pierrefeu [30] failed to measure the flat band potential of the magnetite electrode. It was concluded that the very high concentration of donor densities of magnetite could be the reason for the failure of measuring the FBP, as this notion is based on the assumption that semiconductors have low donor densities in the derivation of Mott-Schottky relations. Freire [34] measured the band gap energy of an *n*-type anodic films formed on iron and on carbon steel. The band gap energy obtained was 2.5 eV, which was close to the 1.9–2.1 eV energy range reported in literature [28]. The value of energy gap was too large for the magnetite, and thus was concluded to be that of other oxide like maghemite or hematite.

3. ELECTROCHEMISTRY OF MAGNETITE

3.1. Adsorption

The charge on (Fe) oxides arises from the preferential adsorption of protons and hydroxyl ions [35, 36], and these are commonly termed potential determining or surface ions. Point of zero charge, the pH at which net adsorptions of potential determining ions on the oxide are zero, is 6.4 for magnetite [35]. OH^- ion is found to strongly adsorb on the magnetite surface [30]. EIS results revealed that OH^- adsorbed on the magnetite much stronger than oxygen**.** With the adsorbed OH^- ions, magnetite surface showed no electrochemical reaction at the open circuit potential. Further evidence of OH^- adsorption was supplied by a Bode type impedance spectroscopy where the impedance and phase angle are obtained against the frequency [30]. In this experiment, at very low frequency of 0.01 Hz, after soaking, the total impedance Z_{mod} increased 10 times that of fresh ME. At high frequencies, Z_{mod} of both cases approached zero. This was understandable, for at high frequencies capacitive components disappear, leaving only pure resistive components. At low frequencies, phase angle also increased by soaking. Increased phase angle meant increased capacitance. These results supported the hypothesis that soaking in 0.1 M LiOH solution for 3 h made magnetite surface covered by OH^-_{ads}, adding capacitive component to the circuit.

Open circuit potential (OCP) evolution of magnetite electrode in 0.1 M LiOH solution under different conditions also supported the adsorption supposition of OH^- on magnetite surface. As anticipated, air-saturated solution raised the potential from the outset. This potential rise was probably coming from the detachment of the adsorbed oxygen, followed by the adsorption of OH^-. OCP also revealed that magnetite electrode adsorbed with OH^- was not easily removed of its adsorbed OH^- layer when dipped into demineralized water. This adsorbed OH^- should already be balanced by positive charges in the magnetite surface, thus showing high potential from the outset of the OCP measurements. When magnetite electrode was pre-immersed in air-saturated, de-ionized water for 21 h, it showed a large potential increase with time when OCP was measured in 0.1 M LiOH. This meant that water molecules were not adsorbing on magnetite surface as OH^- does.

Direct evidence of OH^- adsorption was provided by the acid-base titration [30]. As the powder form of magnetite surely has a much higher surface area than the sintered magnetite electrode surface does, the manufactured magnetite powder (average diameter of 0.6μm) was used for the adsorption experiment.

3.2. Electro-Oxidation

At potentials greater than +0.7V/SCE, oxygen evolution occurred on the surface of magnetite electrode. According to Bagotsky [37], electrochemical oxidation on metals or oxides occurs through the formation of adsorbed oxygen-containing species of the type OH_{ads} or O_{ads} by the discharge of water molecules or OH^- ions. Conclusively, it was suggested that adsorbed OH^- ions on the magnetite surface undergo oxidation via:

$$OH^-_{ads} \rightarrow OH_{ads} + e^- \quad (3)$$

Oxygen generation would follow by the intermediate step such as

$$OH_{ads} + OH_{ads} \rightarrow H_2O + O_{ads} \quad (4)$$

In a specific occasion when the magnetite electrode was immersed in 1M LiOH for a few days, rusts with red colors typical of the hematite were found on the magnetite surface. This observation strongly supported the supposition that magnetite surface itself could easily be oxidized, at least in an aerated, strongly alkaline solution. However, usually in dilute LiOH solutions or in distilled water, magnetite surfaces did not show any sign of rust formation at least after 3 or 4 days of elapse in the open air. At any rate, the EIS result of the magnetite electrode in 0.1 ~ 0.3 M LiOH showed no tendency of electrochemical oxidation, as could be seen by the negligible exchange current density at the electrode [30].

3.3. Electro-Reduction

Magnetite surface adsorbed with ions showed negligible reduction when reductive potential was applied to the magnetite electrode. In an attempt to regenerate the magnetite surface by removing the adsorbed OH^- ions, many cycles of CV were performed. When OH^- was repelled by the negative potential application, reduction became possible. Each successive cycle produced peaks characteristic of fresh ME, i.e., peaks A and B, and resulted in increased peak heights than the previous ones as can be seen in Figure 3. This result showed that magnetite surface can be regenerated after a sufficient number of CV cycles, resulting in the total removal of adsorbed OH^- ions. The large currents at later cycles excluded the possibility of the reduction of magnetite surface.

Some obvious features of the magnetite electrode at strong alkaline solution of 0.1-0.5M LiOH when reducing potential was applied were observed. One is that there appeared two peaks each distanced from one another by a little larger than 0.1V. The second conspicuous one was that each time reductive scan was applied, resultant current increased. This current increase was observed for all the oxidizing currents as well as the reducing currents. The most probable cause of these current increases was supposed to be the electron injection into the energy levels of the magnetite each time potential was applied onto the magnetite electrode: i.e., polarizing towards negative direction possibly resulted in an increase of electron concentration at the conduction band edge (E_C). Contrary to this result, on the platinum in 0.1M LiOH, it was observed that only one reduction peak appeared before the hydrogen evolution. The reason for the one peak appearance on the platinum electrode was self-evident, because platinum as a metal should have only one Fermi level, leading to an appearance of only one reducing signal before the hydrogen evolution.

Apparently, peaks A and D were a reduction-oxidation pair. Even at the slowest scan rate (3mV/s), the peak separation was 0.388V, which was quite large compared to the theoretical value of 0.057V for a reversible pair involving one-electron reaction. Peaks A and D were therefore considered to be totally irreversible with α = 0.36~0.38 and $k_0 = 5.8 \cdot 10^{-5}$ cm/s. Usually, k_0 values lie in 10^{-9}-10 cm/s. The value of k_0 was typical of an irreversible reaction.

As all the peaks A to E shifted to larger overpotentials when the scan rate became faster, plotting peak potentials vs. scan rates for each peak led to peak potentials corresponding to

'zero' scan rate. These potentials were designated as "potential at zero scan (PZS)" for each peak. The PZS was interpreted to be the formal potential of the relevant electrochemical reaction. Plots of peak potentials at various scan rates led to PZS values (all vs. SCE) as -1.06V (A), -1.20V (B), -1.04V (C), -0.75V (D) and -0.58V (E), respectively, for ME in argon-purged 0.3 M LiOH. As peak E was rather difficult to discern, measured peak potentials could contain significant errors for this peak.

As the band gap of magnetite is only about 0.1eV, it was conceived that E_C (conduction band edge) and E_V (valence band edge) were involved in the electrochemical measurements [38]. Thus, water molecule reduction at peak A and then at peak B was plausible. According to this scheme, at potential where peak A appears, electrons drive the reduction as shown schematically in Figure 4. At more negative potential where peak B appears, holes can participate in the reduction. Therefore, peak A was attributed to the reduction of adsorbed H_2O by an electron from E_c:

$$H_2O_{ads} + e^- \rightarrow H_{ads} + OH^- \text{ (Peak A)} \quad (5)$$

Whereas peak B to the reduction by hole transfer to:

$$H_2O_{ads} \rightarrow H_{ads} + OH^- + p^+ \text{ (peak B)} \quad (6)$$

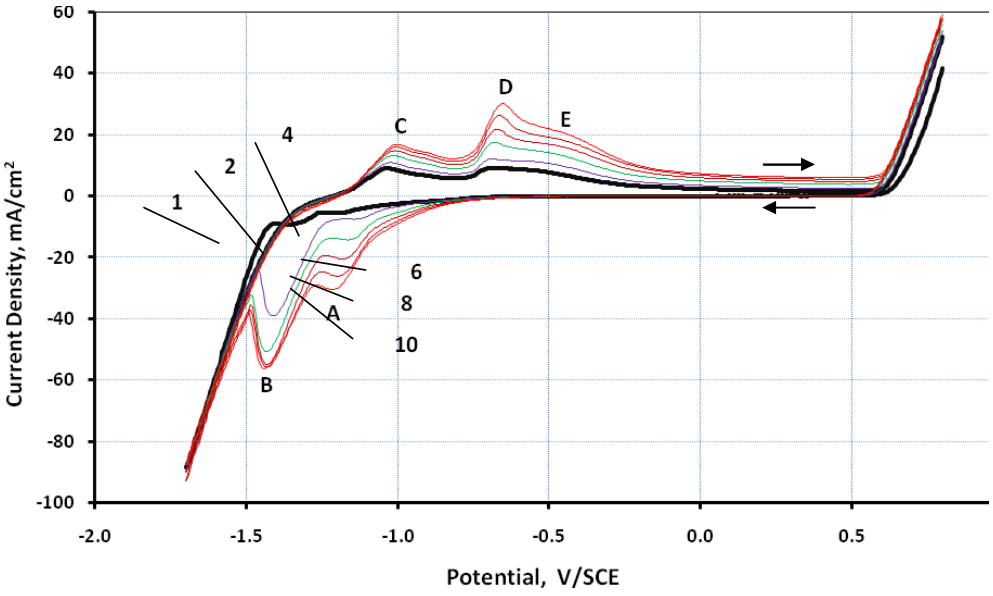

Figure 3. Ten consecutive cyclic voltammograms (CV) of magnetite electrode previously soaked 39 h in 0.1 M LiOH solution. Every second cycle is shown for clarity. Scan rate = 20 mV/s; Ar-purged, 0.5 M LiOH

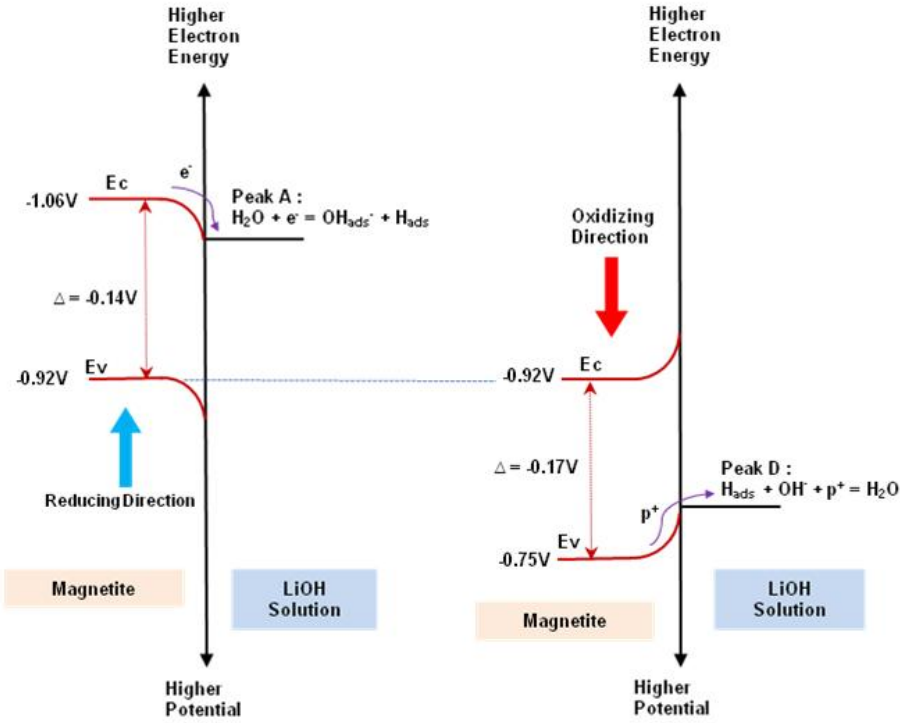

Figure 4. Energy levels and the electrochemical reduction pair A and D as well as pair B and E on the surface of the magnetite electrode

Potential difference (0.14 V) between peaks A and B was concluded to be the band gap E_g between E_C and E_V, in reasonable agreement with the literature value of 0.1 eV [28]. In Figure 4, in the reducing direction, E_v appeared 0.14V below peak A; while in the oxidizing direction, E_c (for peak E) appeared 0.17 V above peak D. These two potential differences coincided at -0.92V on the energy level diagram. In reducing direction, a negative potential applied for peak A to appear will make the energy level curved downward at the surface. Similarly, for oxidizing polarization, when -0.75V for peak D was applied, energy levels will be curved upward at the surface. Potentials for the electrode reactions on the magnetite electrode were concluded to be symmetrically distanced from the flat band potential, with reductions and oxidations occurring at the two band edges, E_C and E_V, and the reactions distanced from each other by $E_G = E_C - E_V$.

Generally, peak C increased when more negative potentials were applied to the magnetite electrode. Thus it was conceived that peak C arose from the oxidation of hydrogen atoms. Oxidation at peak C was suggested to occur through hole acceptance from E_V by the adsorbed hydrogen:

$$H_{ads} + p^+ \rightarrow H_{ads}^+ \tag{7}$$

Hydrogen atoms in the magnetite matrix near the electrode surface also participate in the oxidation alongside H_{ads}. Adsorbed hydrogen ion, with its positive charge, would detach from the surface by reaction with OH^-, producing H_2O.

Results revealed that hydrogen atoms impregnated into the magnetite body during the reductive electrolysis. Actually, when the OCP was measured after the electrolysis, one could see gas bubbles oozing out from the magnetite surface even more than ten minutes after the end of the electrolysis. With this result in mind and considering that peaks D and E forms pairs with peaks A and B, respectively, oxidation of hydrogen was supposed to occur at peaks D and E with the participation of OH^- ions when the polarization went to positive direction:

$$H_{ads} + OH^- + p^+ \rightarrow H_2O_{ads} \text{ (peak D)} \quad (8)$$

$$H_{ads} + OH^- \rightarrow H_2O_{ads} + e^- \text{ (peak E)} \quad (9)$$

4. MAGNETITE AND FLOW ACCELERATED CORROSION (FAC)

4.1. Corrosion of Carbon Steel at High Temperature

In aqueous alkaline solution at high temperature and slightly reducing conditions, magnetite forms as a double-layer on carbon steel surface. The inner layer, next to the metal, is fine-grained (with a grain-size less than 0.1 □m) and grows into the metal as it corrodes. The outer layer consists of solution-grown crystals, generally a few □m across, and grows at the oxide-solution interface [12, 39]. Cook and Lister [12] assumed that the volume of metal corroded in any instant is directly replaced by the oxide that constitutes the inner oxide layer, and they defined this as the metal-oxide (m/o) interface. They also defined the oxide-solution (o/s) interface as top surface of the inner oxide layer or, if coolant conditions permit its existence, the outer layer. At the metal-oxide interface the following redox reactions occurred [12; 40]:

$$Fe \rightarrow Fe^{2+} + 2e \quad (10)$$

$$2H^+ + 2e^- \rightarrow H_2 \quad (11)$$

Approximately one half of the ferrous ions will immediately react and form the magnetite inner layer whilst the remaining ions are available to diffuse to the oxide-solution interface. The precipitation of the magnetite layer generally proceeds through the hydrolysis of ferrous ions to $Fe(OH)_2$, followed by the Schikorr reaction as shown below:

$$3Fe(OH)_2 \rightarrow Fe_3O_4 + 2\,H_2O + H_2 \quad (12)$$

At lower temperatures (303 to 373 K), oxygen is required for the conversion of $Fe(OH)_2$ to magnetite:

$$3\,Fe(OH)_2 + 1/2\,O_2 \rightarrow Fe_3O_4 + 3H_2O \quad (13)$$

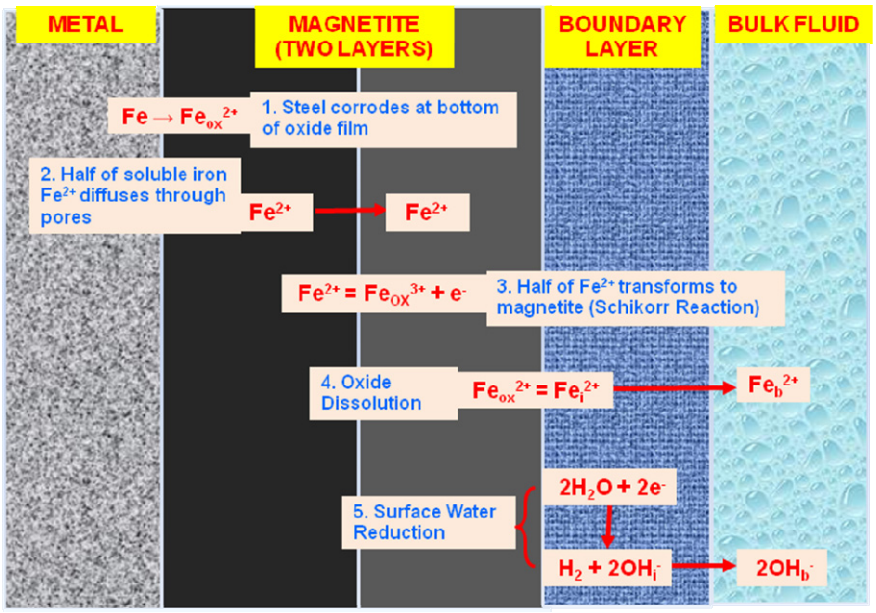

Figure 5. Schematic view of the iron corrosion at high temperature in a reducing condition

The second reaction occurs at all temperatures of interest. And this fact could be a basis for the stifling of FAC by the addition of oxygen into the coolant water. Corroding iron in high temperature coolant waters can be schematically depicted as Figure 5, adopting the idea of Burril and Cheluget [10] and Bignold et al. [41]. In the figure, processes 1~3 can be said to be the iron corrosion. Process 4 is the dissolution of magnetite, which will be covered in the next section. By modeling the corroding surface of iron similar to Figure 5 and formulating appropriate differential equations, Burril and Cheluget [10] estimated that a steady state of carbon steel corrosion reached in 100 hours, after which the oxide film was ~1□m thick.

Bignold dipped iron electrode in deoxygenated 1M NaOH at 238°C for 3 hours, then obtained cyclic voltammetric result referenced to Hg/HgO electrode [8]. The potential from -0.1V to -0.9V was scanned. On the way to negative potential, two reduction peaks at -0.590V and -0.650V were obtained. These two peaks were interpreted to be coming from the reduction of Fe_2O_3 to Fe_3O_4. The reason for the presence of two peaks was not clear, but was conjectured to be coming from the different crystal faces or the reductive dissolution of the oxides like γ-Fe_2O_3 or α-Fe_2O_3. This appearance or two reduction peaks is very similar to Jung and L. de Pierrefeu's result with magnetite electrode which showed two reduction peaks at -1.06V and -1.20V (all vs. SCE, at room temperature). There was however a very different interpretation of the result. While Bignold interpreted the cathodic signals coming from the reduction of Fe_2O_3 to Fe_3O_4, Jung and L. de Pierrefeu interpreted their result as coming from the interaction of H_2O molecules with the energy levels of magnetite. Probably this different interpretation resulted from the different electrode materials as well as the different temperatures: i.e., Bignold used iron as the electrode at 238°C, while Jung and L. de Pierrefeu used sintered magnetite electrode for the electrochemical measurements at room temperature. It will be interesting to examine how the cathodic polarization will be on a magnetite electrode if the temperature were high enough to e that of the coolant.

4.2. Magnetite Dissolution

Several microns-thick magnetite layer may become passivated and protect the metal surface from the corroding species present in the coolant. This normally causes the corrosion rate to drop, now limited by the rate of magnetite dissolution and/or diffusion of iron species through the film [42]. Direct measurement of dissolved iron from the magnetite electrode when various potentials were applied to the electrode was made by Allen, et al. [43]. Their result obtained on the magnetite admixed with carbon paste dipped in the rather acidic solutions at pH 1~3 at 23°C. It was concluded that the iron dissolved into the solution led to the formation of Fe^{2+} ions, thus necessitating the reduction of Fe^{3+} ions in the lattice to make up the Fe^{2+} deficiency. The dissolution rate was concluded to be dependent on potentials applied to the electrode, although a voltage applied to the electrode was not solely distributed on the solid-solution interface, but seen inside the magnetite electrode. This distribution of potentials was attributed to the semiconducting nature of the magnetite. This result was rather contrary to Jung and L. de Pierrefeu's result in the 0.1 ~ 0.3 M LiOH solution [30]. Jung and L. de Pierrefeu's result showed no dissolution of magnetite, but indicated the reduction of water molecules on the magnetite electrode at the reducing potentials. Another cause of the difference can be the different method of making the magnetite electrode: Allen et al. made the electrode admixed with carbon paste, while Jung and L. de Pierrefeu made the electrode by sintering the magnetite powder into a rod-shaped one.

Bignold et al. [41] modeled the dissolving surface of magnetite as a multi-layer where many dissolution-related reactions are taking place. Their layers were a metal-oxide-solution layer as shown in Figure 5. Process 4 in Figure 5 is the dissolution of magnetite, and the full description of the dissolution was depicted as the following reductive dissolution:

$$Fe_3O_4 + 2H_2O + 2H^+ + 2e^- = 3Fe(OH)_2 \quad (14)$$

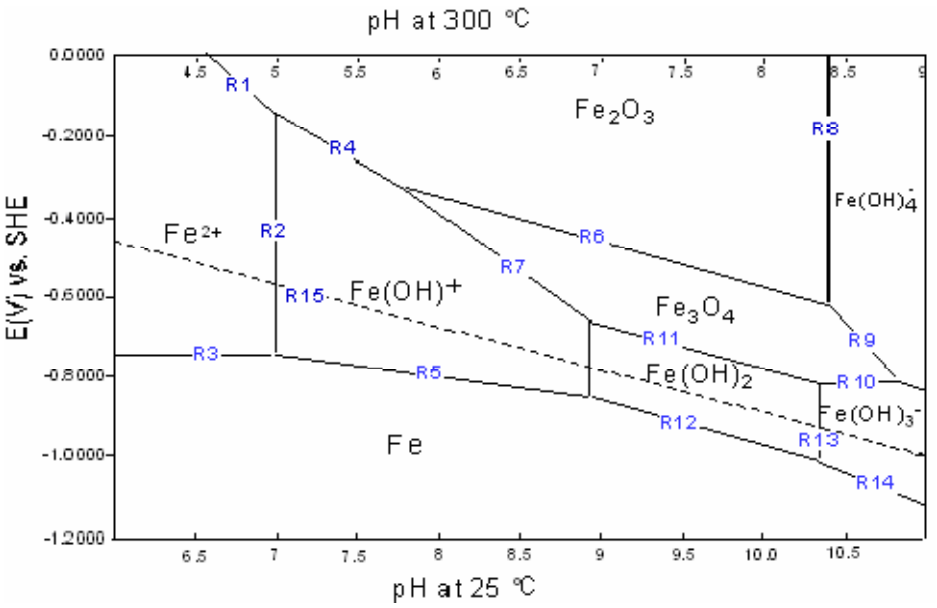

Figure 6. Pourbaix Diagram for Iron in Water at 300°C [42]

Here the electrons necessary for the reduction of magnetite were certainly coming from the transformation of Fe^{2+} to Fe^{3+} that produces electrons in the media. These electrons will then be utilized in the magnetite dissolution and the water reduction on the surface designated as reaction 5 of Figure 4 will occur. Reductive dissolution of magnetite was also predicted by the potential-pH diagram (Pourbaix Diagram) seen in Figure 6 [42].

Bohnsack [44] suggested that magnetite could be regarded as a mixed oxide Fe_2O_3 + FeO, where only the latter is soluble in acid, neutral and slightly basic conditions. The lower stability of the oxygen bridge bond of Fe^{2+} (due to a larger and less charged cation, hence a longer and weaker bond) was considered to explain the solubility equilibrium with divalent iron only. Accordingly, the solubility of Fe^{3+} is 4 to 5 orders lower than that of Fe^{2+}. In strong alkali medium, this argument was no longer valid since trivalent iron becomes soluble to a larger extent, as Tremaine and Leblanc noticed [45].

4.3. FAC in the Power Plant Conditions

An accident occurred (5 Killed, 6 Injured : Aug 2004) at Mihama Power Station, Unit 3, Japan on August 9, 2004 [46]. In this accident, secondary piping ruptured and high temperature cooling water flowed out, so the reactor shut down automatically [Figure 7]. An investigation was carried out on the spot and an opening was confirmed in a pipe of the condensate system. This accident was one of so-called secondary piping rupture accidents of a pressurized water reactor (PWR), and is a typical example of flow accelerated corrosion (FAC) occurring on the carbon steel piping in high temperature coolant systems in nuclear as well as fossil fuel power plants.

FAC causes wall thinning of carbon steel piping, tubing, and vessels exposed to flowing water or wet steam in power plants [11]. The thinning results from dissolution of the normally protective oxide layer (magnetite) that forms on the surface of carbon steels. In fossil plants, most of the serious incidents have occurred when the feedwater was electrochemically reducing. This is caused by the very low levels of oxygen in the presence of a reducing agent (e.g., an oxygen scavenger such as hydrazine).

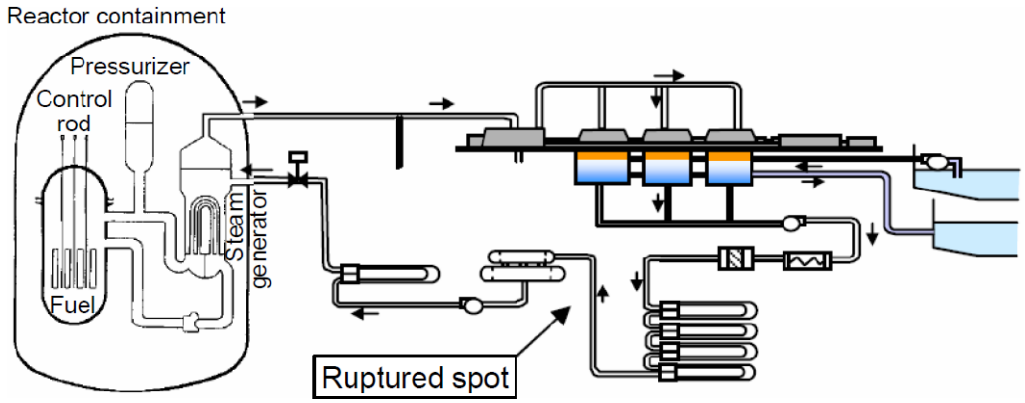

Figure 7. Major systems of PWR and the ruptured spot

In the feeder pipes of the CANDU reactors, the cause of the FAC was also attributed to the under-saturation in dissolved iron with respect to magnetite of the coolant [10]. There is no significant corrosion of inlet feeder pipes because in this region of the reactor the heavy water is super-saturated in dissolved iron. As coolant traverses the core, temperature increases, thus solubility of magnetite increases. So the coolant is unsaturated in dissolved iron at the core exit. There is a driving force for oxide dissolution, leading to corrosion of outlet feeder pipes. At the pH of 10.7, the coolant entering the core at 265°C should be saturated in dissolved iron at about 13 ppb (47). At the reactor outlet, the temperature has risen to 310 °C and the solubility is about 24 ppb. Since there is hardly any source of iron in the core (because the fuel is made mostly of zirconium alloys) the outlet coolant is under-saturated to the extent of 11 ppb and there is a driving force for FAC to occur [48].

The open-circuit potential of carbon steel was lowered during FAC [41]. Chromium alloy steels have much lower FAC rates than mild steel under equivalent conditions. This was attributed to the enrichment of chromium in the corrosion film. Potential decrease arising from FAC may be coming from the generation of electrons by the oxidation of iron constituting the carbon steels.

The cessation of FAC by the addition of oxygen gas leads to an increase in the open-circuit potential of carbon steel several hundred mV [10]. For various potentials, Burril and Cheluget [10] calculated magnetite solubility at temperatures 25°C ~ 300°C. According to their result, solubility of magnetite becomes lower as potential becomes higher. Soluble iron species can be converted to magnetite according to the Schikorr Reaction (12) or (13). Thus presence of oxygen can stifle the FAC. According to these reaction schemes, magnetite dissolution is suppressed by the presence of oxygen, rather than by electrochemical ones.

The details of how dissolved oxygen reacts with oxide films on carbon steel undergoing FAC under feedwater conditions has been investigated by Lister et al [49]. They determined that:

- in neutral, oxygenated water with [O_2] greater than ~40 ppb corrosion was too low to be measured and an electrochemical corrosion potential (ECP) greater than ~-0.25 V (vs.SHE) was measured;
- for ammoniated water, an optimum injection rate of O_2 appropriate for stifling FAC in a feedwater line yet allowing no ingress into the steam generator could be specified;

Khatibi et al. [50] obtained the threshold concentration of O_2 which stifles the FAC. They postulated that for stifling to happen, oxygen has to diffuse through the pores of the magnetite in the oxide film to the oxide-metal interface, and the minimum oxygen concentration in the solution necessary to provide this driving force was essentially the threshold oxygen concentration value for stifling. This minimum oxygen concentration was just enough to react with the Fe^{2+} ions as they are produced. In a specific case of ammoniated chemistry, the oxygen stifling concentration to be 1.2ppb was obtained. Hydrazine levels have continually been reviewed and “optimized”, with due regard to any impact on flow accelerated corrosion (FAC) in secondary systems [51]. Oxygen concentrations have to be maintained above a minimum level to avoid increasing FAC rates in feedwater systems.

5. pH-, ORIFICE-DISTANCE- AND MATERIAL-DEPENDENCY OF FAC

5.1. FAC Mechanism [1]

FAC is a process whereby the normally protective oxide layer on carbon or low-alloy steel dissolves into a stream of flowing water or a water-steam mixture. FAC occurs under both single and two-phase flow conditions. Because water is necessary in order to remove the oxide layer, a FAC does not occur in lines transporting dry or superheated steam.

The FAC process is an extension of the generalized corrosion process of carbon steel in stagnant water. The major difference is the effect of water flow at the oxide-solution interface. A FAC processes are occurring by coupled processes in the porous magnetite layer on the steel surface up to about 300℃ [24].

The first process produces soluble ferrous ions at the oxide-water interface and can be separated into three simultaneous actions:

- Metal oxidation occurs at the iron-magnetite interface in water at a reducing potential;
- The ferrous species diffuse from the iron surface to the main water flow through the porous oxide layer;
- The magnetite oxide layer at the oxide-water interface is dissolved by a reducing process which is promoted by the presence of hydrogen.

The second process involves the transfer of the ferrous ions into the bulk water across the boundary layer. The concentration of ferrous ions in the bulk water is very low compared to the concentration of ferrous ions at the oxide-solution interface. The corrosion rate increases if there is an increase of the water flow past the oxide-water interface. This dissolution process is controlled by the oxidation-reduction potential (ORP) of the water. The more reducing the feedwater is, the higher is the dissolution and the level of the corrosion products in the feedwater.

Under alkaline, deoxygenated (reducing) conditions, the primary reaction of the iron dissolution is inhibited by the increase of pH or by the decrease of reducing environment (i.e. ORP becoming more positive). This causes a reduction of the ferrous ion [Fe^{2+} and $Fe(OH)^{+}$] concentration. The solubility of the ferrous hydroxide ($Fe(OH)_2$) rises with an increasing temperature to a maximum at around 150℃, then decreases with a steep drop to the solubility of the magnetite between 200 and 250℃ [44].

5.2. Experimental Methods[2]

An Erosion-Corrosion Test Loop was designed and constructed as shown in Figure 8. Test specimens were made of carbon steel (A106 Grade B) and low-alloy steels [A336 P11 (1Cr-½Mo) and A335 P22 (2¼Cr-1Mo)], with their chemical composition as shown in Table 1.

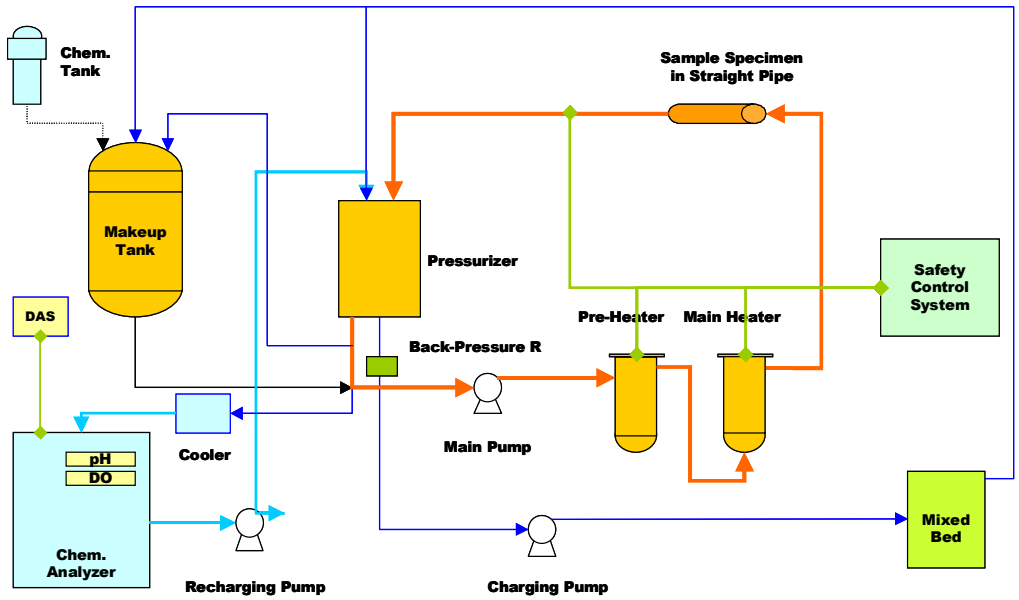

Figure 8. Schematic diagram of an Erosion-Corrosion Test Loop [1]

Table 1. Chemical composition of the test specimens

Mat.	Specification	Chemical Composition (Wt %)								
	(ASTM)	C	Mn	P	S	Si	Ni	Cr	Mo	Fe
1	A106 Gr. B	0.3	0.29~1.06	0.048	0.058	0.1				Balance
	(Commercial)	(0.15)	(0.64)	(0.003)	(0.014)	(0.19)	(0.06)	(0.03)	(0.01)	
2	A336 P11	0.15	0.3~0.6	0.03	0.03	0.5~1.0		1.0~1.5	0.44~0.65	Balance.
	(1Cr-½Mo)	(0.1)	(0.36)	(0.009)	(0.009)	(0.56)		(1.06)	(0.48)	
3	A335 P22	0.15	0.3~0.6	0.03	0.03	0.5		1.9~2.6	0.87~1.13	Balance.
	(2¼Cr-1Mo)	(0.09)	(0.49)	(0.012)	(0.008)	(0.21)		(2.03)	(0.97)	

* Pipe: ID ½", SCH 80 (~3.3 mm in wall thickness)
** Values in parentheses are the actual composition of product

Four ring-typed specimens, of which the inner surface (1.65 cm in inner diameter, 0.375 cm in width) only made contact with the stream, were positioned in a specimen bundle as shown in Figure 9. The four bundles were positioned at the specimen test section in the loop. Three bundles contained an orifice of 6 mm in inner diameter giving a velocity of 4 m/sec, whereas remaining one contained an orifice of 4 mm giving 9 m/sec.

Solution pH and dissolved oxygen (DO) content were measured by using an on-line pH-meter (Omega Co.) and an on-line DO-Analyzer (TOA Electrics Co.), respectively. Surface characteristics of the specimens were observed and analyzed by using a scanning electron microscopy (SEM) (JEOL JSM-6300 Scanning Microscope), a x-ray diffraction (XRD) (Rigaku D/MAX-2000 X-ray Diffractometer) and an x-ray proton spectroscopy (XPS) (XPS LAB MIC II, B.G. Scientific Co.), respectively. Dissolved iron contents sampled after 500 hours were analyzed by using an ICP-AES (Inductively Coupled Plasma–Atomic Emission Spectroscope, IRIS-DUO). Before testing, the external impurities contaminated on the surface

of the ring-typed specimens were ultrasonically cleaned, and the specimens were weighed after a drying.

In order to obtain reasonable weight loss data within at least 500 hours, the experiment was carried out in a DO-free aqueous solution at 130℃, thus providing a maximum FAC rate for carbon steel and low-alloy steels. The solution was de-aerated by a nitrogen gas injection and de-oxygenated by an oxygen-hydrazine reaction. The DO value detected by the on-line DO-meter located at the outlet of the stream passing the test section was maintained at less than 1 ppb, thus ensuring it was DO-free.

The pH controlling agent used was ammonia which is still widely applied to the secondary water chemistry system of PWR nuclear power plants (NPPs). The value of the solution pH was kept at 8.0, 8.5, 9.0, 9.3, 9.43, 9.5, 9.625, 9.75 and 10.0. The surface characteristics and chemical feature of the specimens before and after 500 hours were observed and analyzed by SEM, XPS and XRD, including ICP-AES for a measurement of the concentration of the iron in a solution.

5.3. Characteristics of the Oxide Layer on the Carbon Steel Specimens [1]

SEM micrographs of carbon steel after 500 hours at pH 9.0 under a flow velocity of 4 m/sec at 20.4 mm from the orifice in the oxygen-free aqueous solution at 130℃ is shown in Figure 10. The non-tested surface is also shown. Usually, general corrosion is accompanied with a lower energy transfer rather than by mechanical damage, and FAC generally shows some traces such as a groove, ripple, gully or thin pitting form [2]. In this study, the tested specimen showed mainly some groove formed due to the fluid flow from left to right. The low-alloy steel specimens showed similar features in the carbon steel.

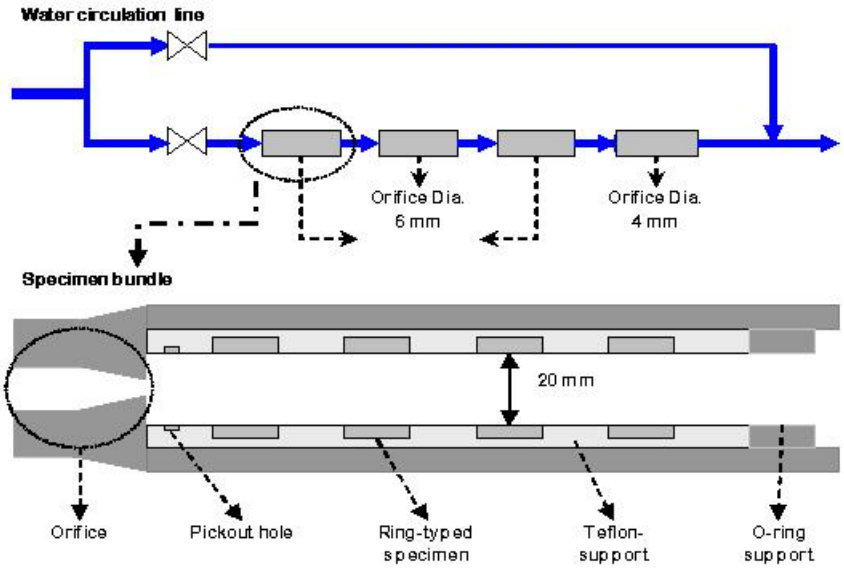

Figure 9. Schematic diagram of the Erosion-Corrosion Test Specimen [1]

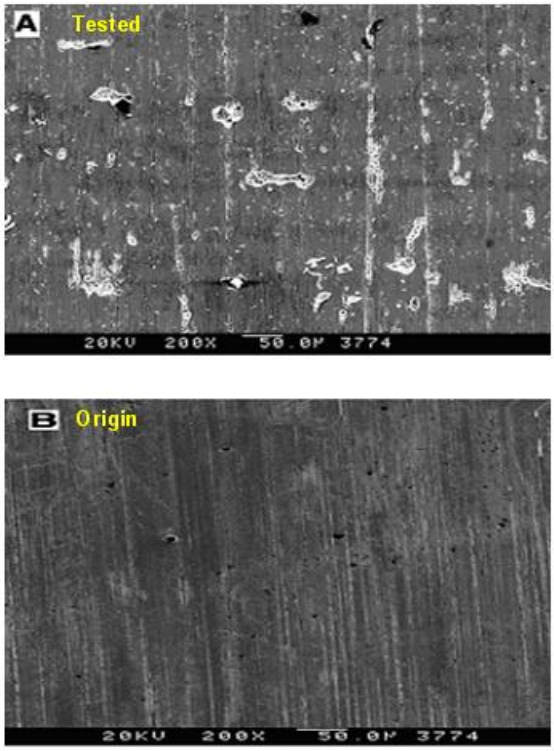

Figure 10. SEM micrographs of carbon steel (CS) after 500 hours at pH 9.0 at the flow velocity of 4 m/sec (A), and the as-received surface (B) [1]

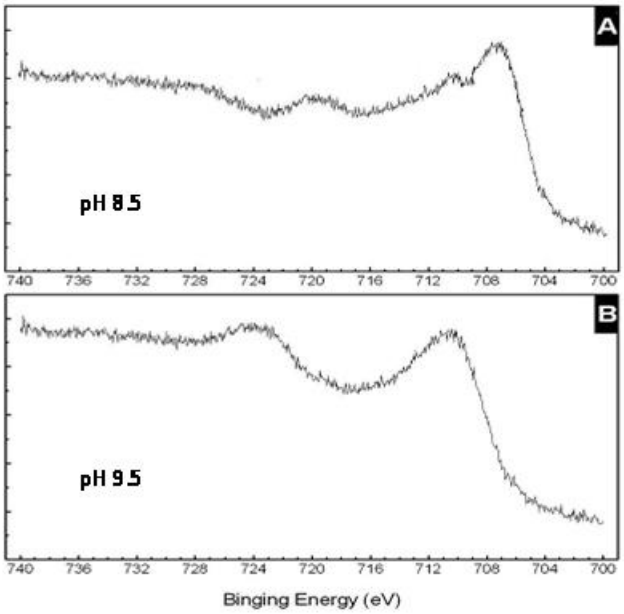

Figure 11. Fe_{2p} XPS spectrum of Fe_3O_4 formed on the carbon steel (CS) after 500 hours at pH 8.5 (A) and 9.5 (B) under the flow velocity of 4 m/sec

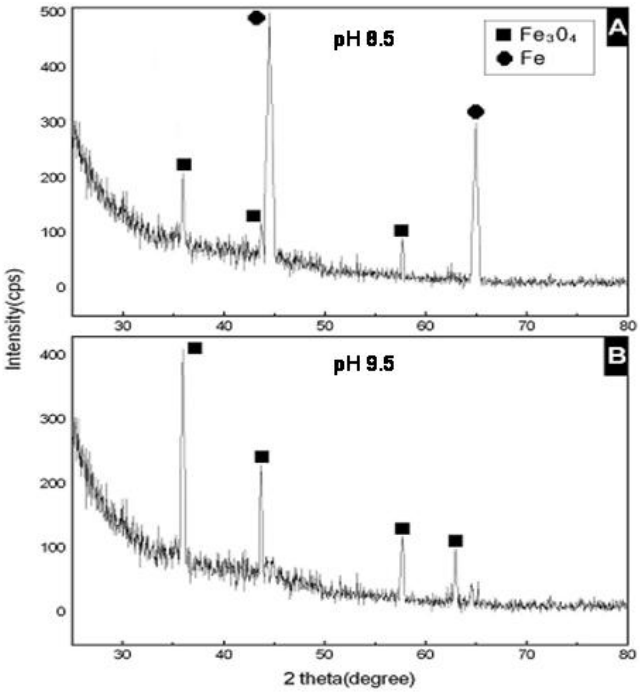

Figure 12. XRD patterns of the carbon steel at pH 8.50 (A) and 9.50 (B) at 130℃ under the flow velocity of 4 m/sec

Fe_{2p} XPS spectra of Fe_3O_4 formed on the carbon steel specimens after 500 hours at pH 8.5 and 9.5 under a flow velocity of 4 m/sec at 20.4 mm from the orifice at 130℃ are shown in Figure 11. The Fe_{2p} XPS spectrum gave the characteristic peak of Fe_3O_4 at a binding energy of 710.4 eV, and that of Fe at 707.0 eV. These peaks showed that the surface of the carbon steel specimen obtained at pH 8.5 contained less magnetite and more iron than those obtained at pH 9.5.

This tendency was also confirmed by the XRD patterns of the carbon steel specimen at pH 8.5 and at pH 9.5 as shown in Figure 12. Two strong peaks of Fe at 2Θ degree of 44.5 and 65.0, including another four weak peaks of Fe_3O_4 at the rest peaks marked in this figure, appeared to be higher for the specimen obtained at pH 8.5 than at pH 9.5. This means that the magnetite dissolution rate at the pH of 8.5 was higher than that at pH 9.5, showing the dependency of FAC of carbon steel on pH and magnetite solubility [25].

5.4. Effect of Flow Velocity on Weight Loss of Carbon Steel [1]

Figure 13 shows the weight loss of carbon steel specimens after 500 hours under the flow velocities of 4 and 9 m/sec at 20.4 mm from the orifice and 130℃ in the pH range of 8.0~10.0. There is a flow velocity dependency of weight loss due to the FAC on carbon steel. The weight loss obtained at a flow velocity of 9 m/sec is approximately 30% higher than that obtained under 4 m/sec. A significant decrease in weight loss of carbon steel at pH 9.5 can be explained by the solubility of iron oxide as a function of pH described below.

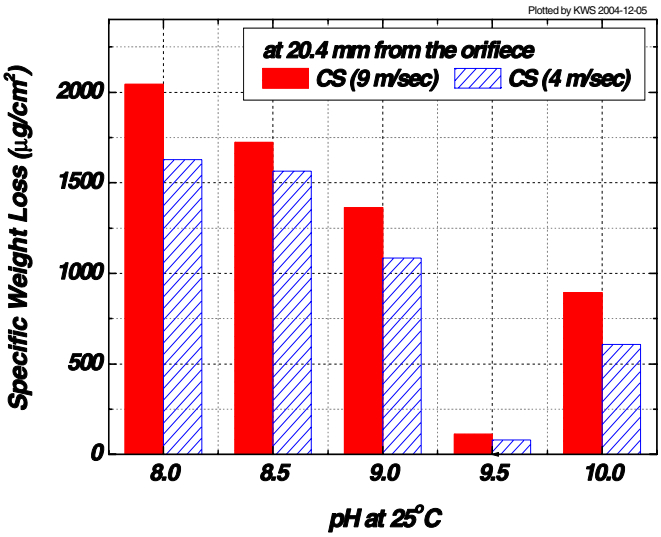

Figure 13. Weight loss of the carbon steel after 500 hours at 20.4 mm from the orifice, dependent under the flow velocities of 4 and 9 m/sec

5.5. Effect of pH on Weight Loss of Carbon Steel and Low-Alloy Steels [1]

As shown in Figure 14, the weight loss of specimens of carbon steel and low-alloy steels (P11: 1Cr-½Mo, P22: 2¼Cr-1Mo) after 500 hours at a pH of 8.0~10.0 under a flow velocity of 4 m/sec and 9 m/sec at 20.4 mm from the orifice and 130℃ is dependent on the pH and material. The weight loss appeared to decrease with increasing pH in the range of 8.0~9.5. While, in the pH range of 9.5~ 10.0, the weight loss inversely increased, showing a minimum at a pH of about 9.5.

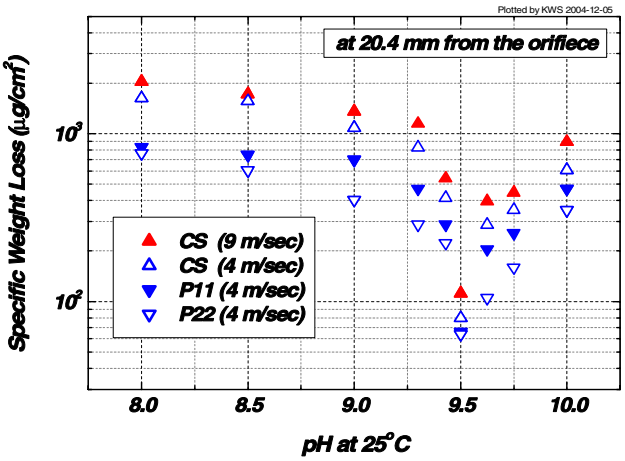

Figure 14. Weight loss of the specimens of carbon steel (CS) and low-alloy steels (P11: 1Cr-½Mo, P22: 2¼Cr-1Mo) at 20.4 mm from the orifice, dependent on the pH and material at 130℃ after 500 hours [1]

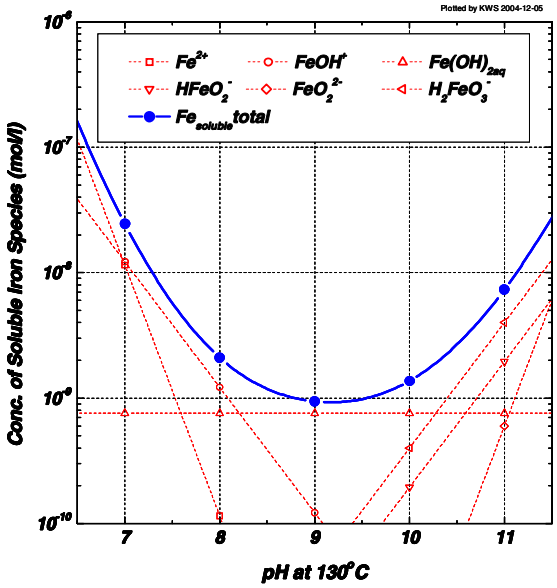

Figure 15. Contributions of the individual soluble iron species to the total magnetite solubility in an aqueous solution, calculated at 130℃, dependent on pH [1]

The most commonly accepted mechanism of FAC in carbon steel and low-alloy steels in a deoxygenated water flowing at a high flow rate at a high temperature is that chemically reductive dissolution of the magnetite (Fe_3O_4) film occurs by an enhanced mass transport of the soluble iron species.

In order to confirm the magnetite solubility effect on the experimental weight loss, the concentrations of the soluble iron species dissolved from magnetite, such as Fe^{2+}, $FeOH^+$, $Fe(OH)_{2aq}$, $HFeO_2^-$, FeO_2^{2-} and $H_2FeO_3^-$, and the total soluble iron, were thermodynamically calculated at 130℃. For the calculation, the following reactions were used with the thermodynamic values obtained from literature [26]:

$$Fe_3O_4 + 2H^+ = 2FeOOH + Fe^+ \quad (15)$$

$$Fe_3O_4 + H^+ + H_2O = 2FeOOH + FeOH^+ \quad (16)$$

$$Fe_3O_4 + 2H_2O = 2FeOOH + Fe(OH)_{2aq} \quad (17)$$

$$Fe_3O_4 + 2H_2O = 2FeOOH + HFeO_2^- + H^+ \quad (18)$$

$$Fe_3O_4 + 2H_2O = 2FeOOH + FeO_2^{2-} + 2H^+ \quad (19)$$

$$Fe_3O_4 + H_2O = H_2FeO_3^- + H^+ \quad (20)$$

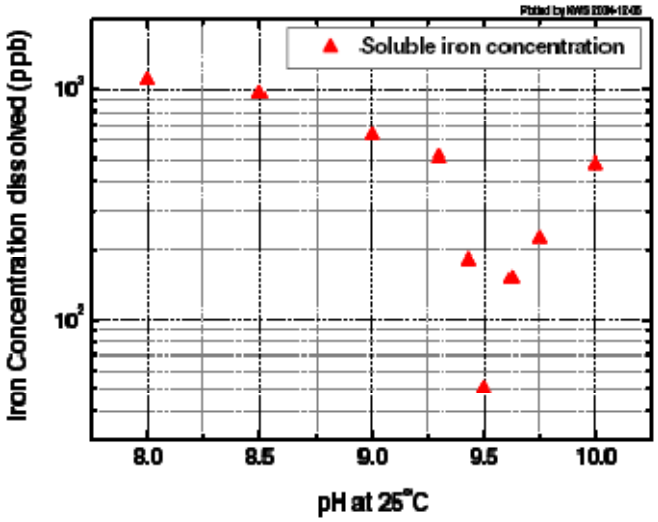

Figure 16. Dissolved iron concentration in the aqueous solution of the test loop at pH

The calculated results are plotted in Figure 15. In the pH range of 8.0~9.5, the reactions that predominantly contributed to the total soluble iron concentration at 130℃ were shown to be the reactions of (1), (2) and (3). While, in the pH range of 9.5~10.0, they were the reactions of (4), (5) and (6). The pH dependency of the magnetite dissolution obtained from the calculation seemed to be consistent with the experimental weight loss results, and with the soluble iron concentration experimentally obtained by ICP-AES, as shown in Figure 16. This means that, under these experimental conditions, the FAC of the carbon steel and the low-alloy steels depended on the magnetite solubility.

There is very little reference in the literature on effect of pH on FAC of the carbon steel and low-alloy steels. The water chemistry personnel at the NPP utility should carefully consider this kind of pH dependency in pH control of the water system for a better mitigation of the FAC of the piping material.

5.6. Effect of Orifice Distance on Weight Loss of Carbon Steel and Low-Alloy Steels [1]

In this experiment, specimens of carbon steel and low-alloy steels were laid out at positions of 6.8, 13.6, 20.4 and 27.2 mm from the orifice in a specimen bundle, as shown in Figure 9. In Figure 17 are plotted the weight loss of carbon steel, P11 and P22 steels as a function of pH and distance from the orifice. A clear dependency of FAC on pH and distance is observed.

The orifice distance dependency was re-plotted at pH 9.0 after a regression, as shown in Figure 18. The weight loss of carbon steel and P11 specimens increased with increasing the distance of the specimen from the orifice. P22 specimens did not show any orifice distance dependency.

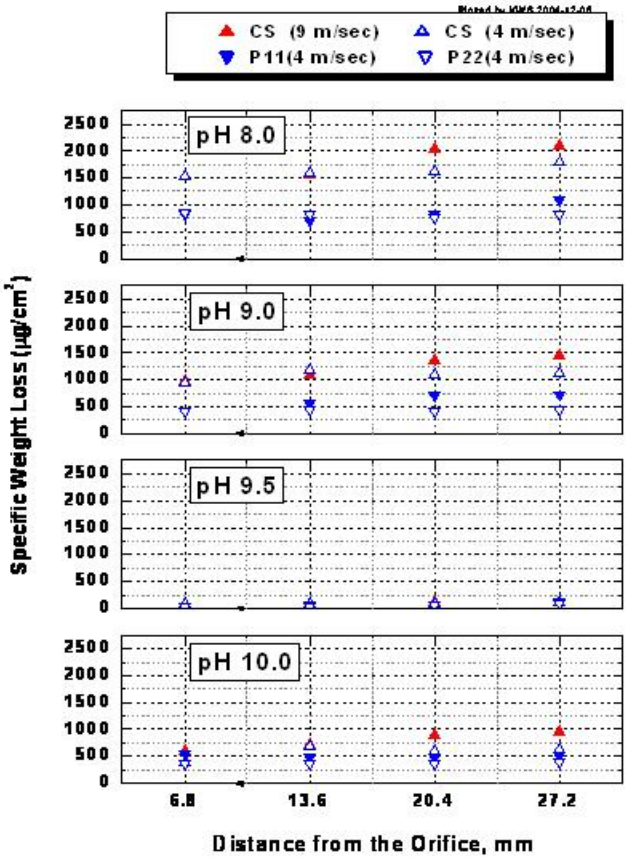

Figure 17. Weight loss of the specimens of carbon steel (CS) and low-alloy steels (P11, P22) at pH 8.0, 9.0, 9.5 and 10.0, dependent on the materials at 130℃ after 500 hours, versus the distance from the orifice [1]

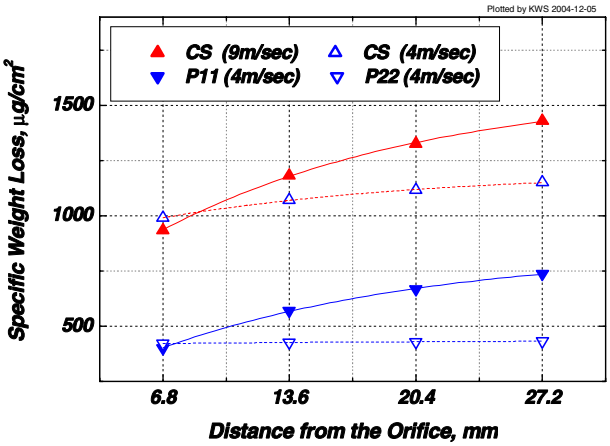

Figure 18. Regression curves of the weight loss of CS, P11 and P22 after 500 hours at pH 9.0 and 130℃ as a function of orifice. distance [1]

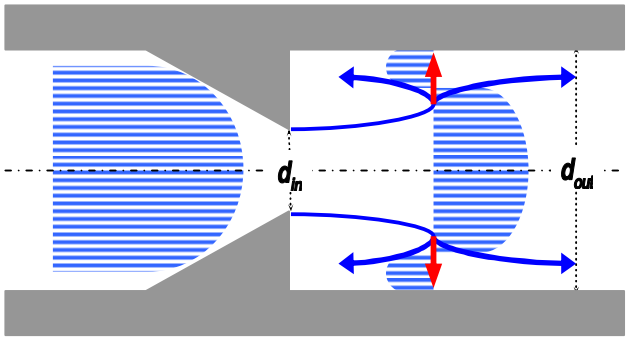

Figure 19. Turbulent pipe with separation (complex velocity field with reverse flow) [1]

This phenomenon was thought to be due to the laminar and turbulent flow that is generated just after passing the orifice, forming a complex velocity with a reverse flow, as shown in Figure 19. In other words, at a certain distance from an orifice at high flow velocity, a pipe would be damaged more by a FAC than at other locations. In order to prevent the kind of pipe rupture shown in Figure 2, it is necessary for the surface, thickness and material of the piping system located at certain plant-specific distance from an orifice to be reconsidered.

5.7. Effect of Material on Weight Loss of Carbon Steel and Low-Alloy Steels [1]

Figure 18 shows the effect of material on the weight loss of the specimens. This figure also shows that the weight loss of carbon steel specimens at flow velocities of 9 and 4 m/sec, and of the P11 specimens at 4 m/sec, at 20.4 mm from the orifice, were shown to be greater than that of the P22 specimens.

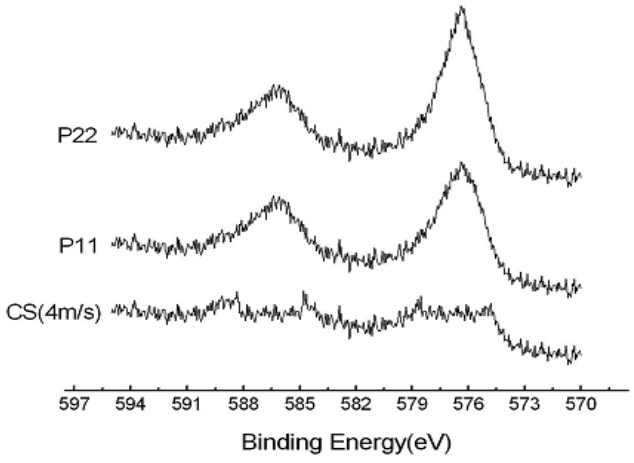

Figure 20. Cr_{2p} XPS spectrum in Cr_2O_3 formed on carbon steel and low-alloy steels (P11 and P22) after 500 hours at pH 9.75 under the flow velocity of 4 m/sec [1]

This material dependency of the weight loss is also shown in Figure 20. This figure shows the Cr_{2p} XPS spectra in Cr_2O_3 formed on the surfaces of the specimens of carbon steel and low-alloy steels (P11 and P22) after 500 hours at pH 9.75 at flow velocity of 4 m/sec. It was found that the steels containing more chromium (P11 and P22) exhibited approximately half the weight loss of that of carbon steel.

Furthermore, as shown in Figure 21, the XRD patterns of the carbon steel showed three strong peaks of Fe_3O_4 at 2θ degree of 36.0, 43.5 and 57.5, but no peaks of Cr_2O_3. Meanwhile, the P11 or the P22 showed strong peaks of Cr_2O_3 at a 2θ degree of 33.0, including some weak peaks of Fe_3O_4, suggesting the coexistence of both Fe_3O_4 and Cr_2O_3.

The chromium contained in the molecular matrix of the specimens of the P11 (1Cr-½Mo) and P22 (2¼Cr-1Mo) was thought to be formed as a non-stoichiometric spinel, $Fe_xCr_yFe_{2-x-y}O_4$, with a very high stability due to its extremely low solubility in the high temperature aqueous solution. In other words, the VI-B transition elements such as Cr (and Mo) added into the carbon steel matrix gave excellent resistance against FAC at approximately two times higher than that of the original one, at a low alkaline pH, as shown in Figure 22.

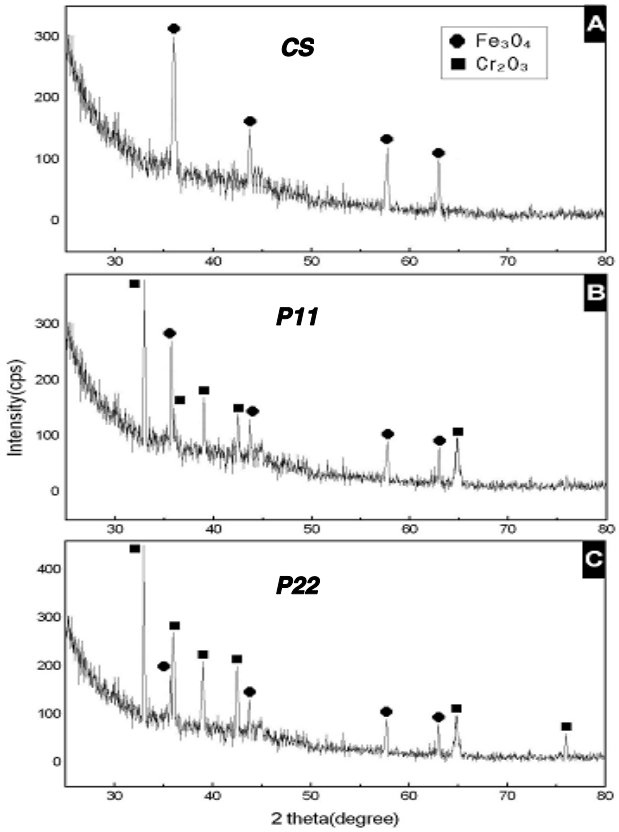

Figure 21. X-ray diffraction patterns of carbon steel (A), P11 (B) and P22 (C) after 500 hours at pH 9.75 and 130℃ under the flow velocity of 4 m/sec [1]

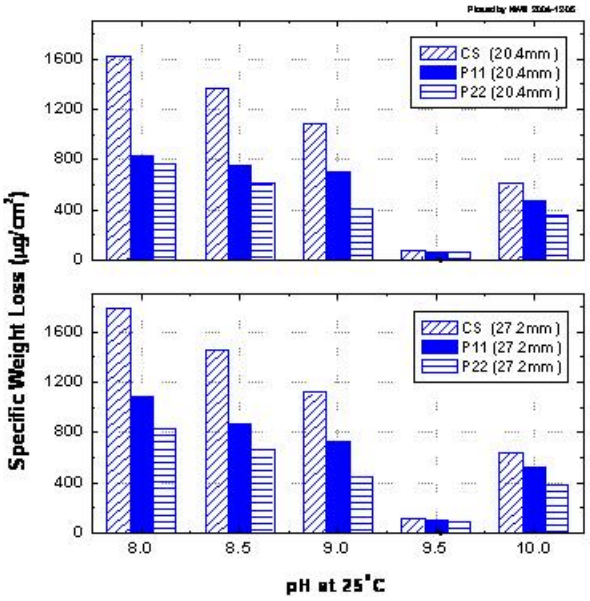

Figure 22. Weight loss of specimens of CS, P11 and P22 after 500 hours at 20.4 and 27.2 mm from the orifice and 130℃, showing dependence on the material [1]

In order to compare the resistance against FAC of the carbon steel and the low alloy steels, the values of the coefficient and the constant of a linear weight loss-pH equation was regressed as the following:

$$WL_{regressed} = A \times pH + B \tag{21}$$

Here, $WL_{regressed}$ is the regressed weight loss, A is the coefficient of the pH dependence, and B is the constant of the linearly regressed equation. The values are presented in Table 2, and plotted in Figure 23. In the range of pH from 8.0 to 9.5 and from 9.5 to 10.0, respectively, the values of A and B were shown to be distinguishably different, depending on the materials. The values of A and B might suggest an index of the pH and material dependency of a FAC of the carbon steel and the low-alloy steels that would illustrate sensitivity to FAC.

Table 2. The constant values of WL (Regressed weight loss (μg/cm²)) = A x pH + B for linear curve fitting [1]

Material	WL (Regressed weight loss (μg/cm²)) = A x pH + B			
	pH 8.0~9.5		pH 9.5~10	
	A	B	A	B
CS 9m/s	-1,190	11,770	1,265	-11,793
CS 4m/s	-1,013	9,973	838	-7,785
P11 4m/s	-473	4,732	670	-6,242
P22 4m/s	-455	4,446	525	-4,924

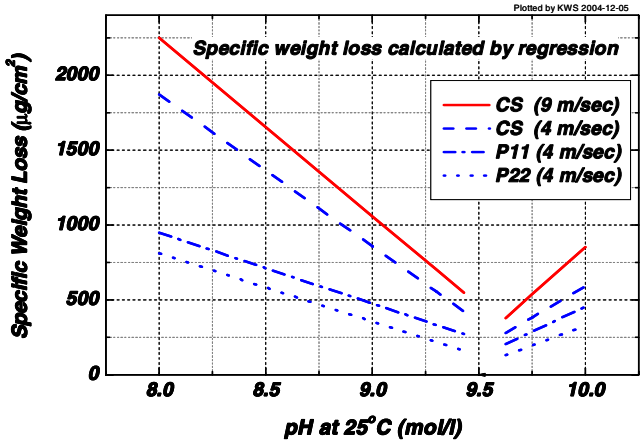

Figure 23. Regression curves of the weight loss of CS, P11 and P22 at 20.4 mm from the orifice at 130℃, showing dependence on the material [1]

Based on this material dependency, it was thought to be desirable to change the material composition of the secondary piping system of the NPPs, with that of the low-alloy steels such as 2¼Cr-1Mo. This could be done when a secondary piping system material is designed for a new NPP construction, and particularly when an old pipe system has to be replaced after an accident like that shown in Figure 2.

6. HYDRAZINE-CONCENTRATION DEPENDENCY OF FAC

6.1. Experimental Methods [2]

A FAC test loop containing an autoclave (200 mm in height, 208 mm in inner diameter) was designed and manufactured as shown in Figures 24 and 25. Six flat specimens (17.8 mm both in length and in width, respectively) made of carbon steel were laid out inside a cylindrical specimen support, and weighed for a weight loss measurement.

A magnetically driven rotating blade inside the specimen support provided the surface of the test specimens with a flow velocity of approximately 8.6 m/sec computer-simulated at a rotating speed of 1500 rpm.

Solution $pH_{25℃}$ was controlled with ammonia, frequently monitored by using a pH-meter (Orion 520A) and kept at 9. Hydrazine concentration was analyzed by using a UV spectroscope (HP 8452) and maintained at 50, 100, 150 and 250 ppb, respectively. Dissolved oxygen concentration was monitored by using an on-line monitor (Dissolve Oxygen Analyzer, TOA DO-30A), and maintained at below 1 ppb. The FAC testing was carried out under a hydrazine concentration of 0, 50, 100, 150 and 250 ppb, respectively, as shown in Table 3.

Recently, the current tests have been carried out at a hydrazine concentration of 500 ppb. The testing was undertaken in a deoxygenated aqueous solution re-circulated in the FAC test loop at an ammonia-controlled pH at 25℃ of 9.0 with a rotating velocity of 1500 rpm at 250℃ for 300 hours.

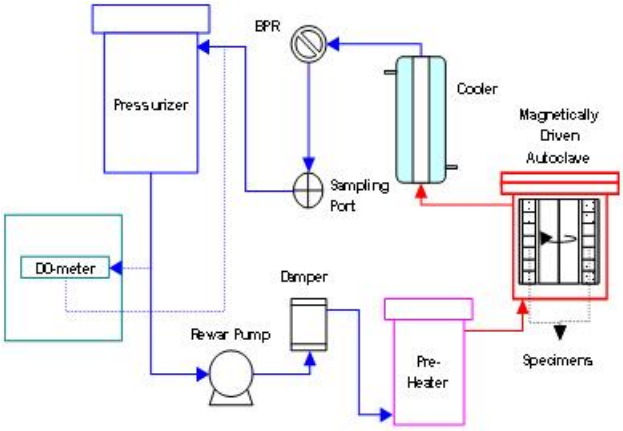

Figure 24. Schematic diagram of the High-Temperature FAC Test Loop [2]

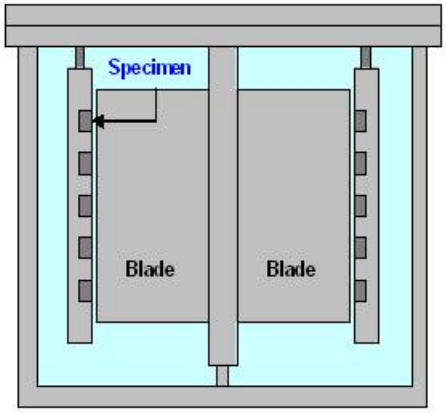

Figure 25. A four- blade and a cylindrical support with the specimens [2]

Table 3. Scheme of the carbon steel FAC testing with hydrazine concentration (the test under 500 ppb is currently being carried out) [2]

N_2H_4 Temp.	0 ppb	50 ppb	100 ppb	150 ppb	250 ppb	500 ppb
250℃	√	√	√	√	√	-

6.2. Effect of Hydrazine Concentration on Weight Loss of Carbon Steel [2]

Figure 26 shows a specific experimental weight loss of the carbon steel specimens in a deoxygenated aqueous solution re-circulated in a FAC test loop at an ammonia-controlled pH at 25℃ of 9.0 at 250℃ with a rotating velocity of 1500 rpm for 300 hours. The average specific weight loss obtained with the hydrazine concentrations of 0, 50, 100, 150 and 250 ppb was approximately 651, 742, 679, 410 and 458 $\mu g/cm^2$, respectively.

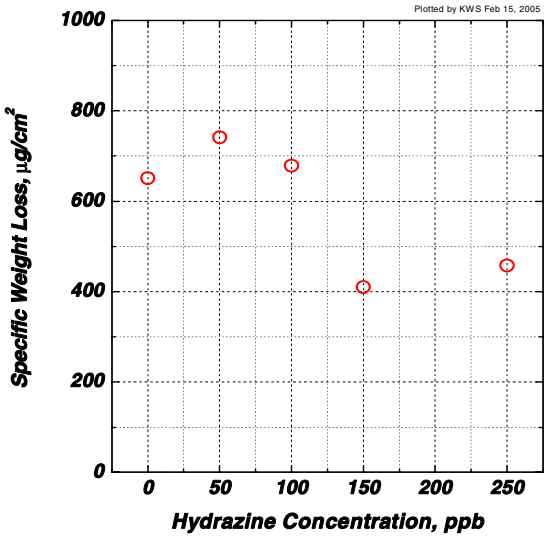

Figure 26. Specific weight loss of the carbon steel specimens in a deoxygenated aqueous solution re-circulated in a FAC test loop at an ammonia-controlled $pH_{25℃}$ of 9.0 at 250℃ for 300 hours [2]

The weight loss of the carbon steel specimens at the hydrazine concentrations of 0~100 ppb appeared to be a little higher than those at 150 and 250 ppb. Figure 27 shows the relative specific weight loss of the carbon steel specimens in a deoxygenated aqueous solution re-circulated in a FAC test loop at an ammonia-controlled pH at 25℃ of 9.0 at 250℃ with a rotating velocity of 1500 rpm for 300 hours.

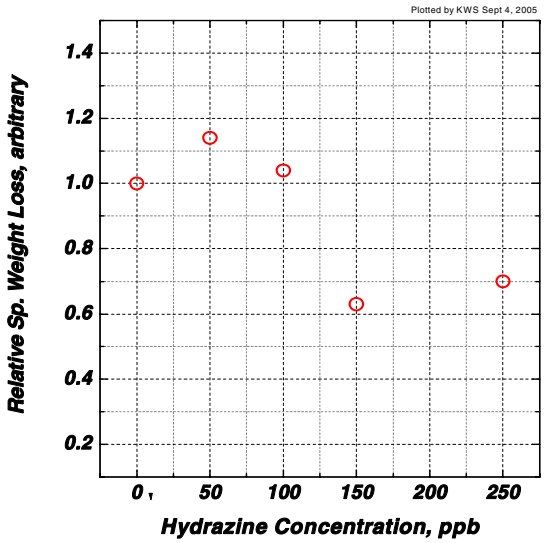

Figure 27. Relative specific weight loss of the carbon steel specimens in a deoxygenated aqueous solution re-circulated in a FAC test loop at an ammonia-controlled pH at 25℃ of 9.0 at 250℃ for 300 hours [2]

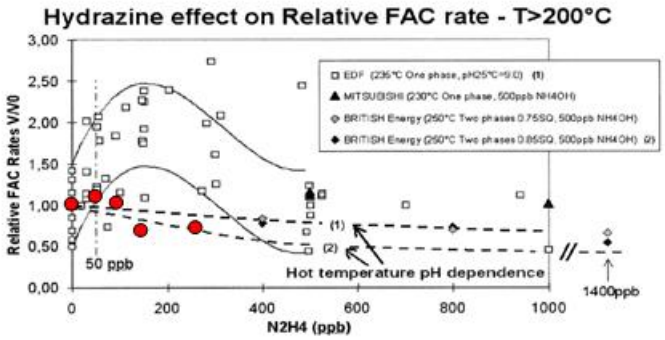

Figure 28. Comparison of the relative FAC rate of carbon steel between the KAERI data (red circles) at 250℃ and the EdF data at 235℃, dependent on the hydrazine concentration with DO < 5 μg/kg [2]

The relative specific weight loss obtained with the hydrazine concentrations of 0, 50, 100, 150 and 250 ppb was approximately 1.0, 1.14, 1.04, 0.63 and 0.70, respectively. These results showed the hydrazine concentration dependency of a carbon steel FAC in this range, having a maximum at a concentration of 50 ppb. This tendency is a little different from that obtained from the EdF data, as shown in Figure 28. More studies on the hydrazine concentration dependency of a carbon steel FAC will be needed.

CONCLUSION

Electrochemical properties of magnetite in alkaline solutions in an ambient temperature were introduced. Some conspicuous characteristics are the adsorption of OH^- ions on the magnetite surface, reduction of H_2O molecules at the magnetite surface in the reducing polarization by interaction with energy levels of magnetite, generation of H atoms at the magnetite surface when negative polarization was made. As the band gap of magnetite (0.14 eV) found to be only about 5~6 times larger than the ordinary thermal energy (0.025eV), it is suggested that magnetite electrode is already strongly influenced by the room light. This band gap of the magnetite is equivalent to $1130cm^{-1}$ which corresponds IR-C region. It is probable that if a suitable circuit was contrived, e.g. with a conductor for the circuit completion, then a solar energy conversion can be possible by magnetite-conductor combination, with/without electrolyte between electrodes. Another possibility is hydrogen generation by electrolysis on the magnetite electrode combined with another suitable electrode. However, preliminary experiments dealing with these ideas showed no promising results. Research results on magnetite electrode at high temperatures of other researchers were discrepant from the above conclusions made at ambient temperatures.

In relation to FAC, many research results were made emphasizing pH and the electrochemical corrosion potential. Causes of the FAC of the carbon steel pipes at the secondary coolant circulating systems of any power plant operations are the under-saturation of iron at the reducing conditions. Thus stifling of magnetite dissolution by raising the potential with the addition of oxygen seems to be a good remedy for FAC. Another alternative for the mitigation of FAC could be the addition of metal ions like Zn^{2+} which forms highly resistive spinel oxides when substituted into the magnetite structure.

In order to investigate the dependency of FAC of carbon steel and low-alloy steels [P11 (1Cr-½Mo) and P22 (2¼Cr-1Mo)], on pH, orifice distance and material, experiments were carried out under flow velocities of 4 m/sec and 9 m/sec in the pH range of 8.0~10.0 in a dissolved oxygen-free aqueous solution re-circulated in an Erosion-Corrosion Test Loop at 130℃ for 500 hours:

- The weight loss of carbon steel appeared to increase with flow velocity.
- The weight loss of the specimens of carbon and low-alloy steels was shown to be distinguishably dependent on pH. In the range of pH from 8.0 to 9.5, it decreased, but increased from 9.5 to 10.0. There is very little reference in the literature about this kind of pH dependency of FAC of carbon and low-alloy steels. Utility water chemistry personnel should carefully consider control of pH of the system water for enhanced mitigation of FAC.
- The weight loss of specimens of carbon and low-alloy steels located further from the orifice was shown to increase within the distance range from 6.8 to 27.2 mm. In order to prevent possible piping ruptures, as shown in Fig. 2, it is recommended that the surface, thickness and material of a piping system located at a certain plant-specific distance from an orifice have to carefully be reconsidered.
- This study also showed that low alloy steels had two times better resistance against FAC than that of carbon steel. Based on this result, it would be necessary to alternate the composition of the secondary piping system material of the NPPs, with low-alloy steels such as 2¼Cr-1Mo, particularly when old system pipes have to be replaced.

On the other hand, an experiment was carried out on the effect of the hydrazine concentration on a carbon steel FAC at $pH_{25℃}$ of 9.0 controlled with ammonia in a deoxygenated aqueous solution re-circulated in a FAC test loop at 250℃ for 300 hours:

- The loop provided a flow velocity by a magnetically driven rotating blade onto the surface of the test specimens located outside of it, at a rotating speed of 1500 rpm.
- The relative FAC rate obtained with the hydrazine concentrations of 0, 50, 100, 150 and 250 ppb was approximately 1.0, 1.14, 1.04, 0.63 and 0.70, respectively.
- These results showed the hydrazine concentration dependency of carbon steel FAC in this concentration range, appearing at a maximum at a concentration of 50 ppb.
- This tendency is a little different from that of the EdF data.

ACKNOWLEDEMENT

The authors are grateful for the resources kindly offered by Dr D. H. Lister and his team of UNB Nuclear, University of New Brunswick for this article.

REFERENCES

[1] Jeong Ho Moon, Hung Ho Chung, Ki Woung Sung and Uh Chul Kim, "Dependency of Single-Phase FAC of Carbon and Low-Alloy Steels for NPP System Piping on pH, Orifice Distance and Material", *Nuclear Engineering and Technology, Vol. 37*, No 4, p. 375~384, August 2005.

[2] Ki Woung Sung, Hyun Il Seo, Jeong Ho Moon, Yong-Moo Cheong and Uh Chul Kim, "*Hydrazine Concentration Dependency of Carbon Steel FAC at pH 9 and 250℃*", Fontevraud 6 International Symposium, France, September 19, 2006

[3] Dobson, D. C., Linnet, J. W. & Rahman, M. M. (1970). *J. Phys. Chem. Solids*, *31*, 2727-2733.

[4] Itai, R., Shibuya, M., Matsumura, T. & Ishi, G. (1971). *J. Electrochem. Soc*., *118*, 1709.

[5] Allen, P. D., Hampson, N. A. & Bignold, G. J. (1979). *J. Electroanal. Chem*., *99*, 299~309.

[6] Allen, P. D., Hampson, N. A., Tyson, J. F. & Bignold, G. J. (1979). *Surface Technology*, *9*, 395~400.

[7] Buchler, M., Schmuki, P., Bohni, H., Stenberg, T. & Mantyla, T. (1998). *J. Electrochem. Soc*., *145(2)*, 373–385.

[8] Bignold, G. J. (1976). "*Observations and Theories concerning the Iron Electrode in Sodium Hydroxide Solutions at 200 to 250˚C",* International Corrosion Conference Series, 499~507.

[9] Wielant, J., Goossens, V., Hausbrand, R. & Terryn, H. (2007). *Electrochimica Acta*, *52*, 7617–7625.

[10] Burrill, K. A. & Cheluget, E. L. (1998). "*Corrosion of CANDU Outlet Feeder pipes",* JAIF International Conf. on Water Chemistry in Nuclear Power Plants, Proceedings, Nov.,

[11] Tilley, R. M., Dooley, R. B. & Brett, C. R. (1998). "*Recent developments in Managing Flow-Accelerated Corrosion in Feedwater Pipework for Fossil-Fired Power Plants",* PVP- *Vol. 380*, ASME.

[12] Cook, W. G., Lister, D. H. (2004). *"Some aspects of electrochemistry and corrosion mechanisms influencing flow assisted corrosion in CANDU outlet feeder pipes"*, Proceedings of the International Conference on Water Chemistry of Nuclear Reactor Systems – CD, San Francisco, October.

[13] Lister, D. H. (1987). *Corrosion Science*, *27(2)*, 113-149.

[14] Shah (1999). "*Flow-Accelerated Corrosion of PWR Carbon Steel Components*", Symposium on Life Extension and Aging Management of Nuclear Power Plant Components in Korea, Korea Institute of Nuclear Safety, Taejon, Korea, July

[15] Kunze, & Nowak, J. (1982). "*Erosion Corrosion Damage in Steam Boiler*", Werkstoffe und Korrosion, *33*, 262~273.

[16] "Accident (2004). at the Kansai Electric's Mihama-3 NPS", *JAIF Focus*, Japan Atomic Industrial Forum, Inc., August 10

[17] Marta, U. (1998). Gmurczyk, Aaron Barkatt, David Ballard, Galina Cherepakhov, William Kessler and Reynolds Burns, "*Identification of corrosion modes in steam pipes from the secondary system at Indian Point 2*", Corrosion 98, paper No. 130, National Association for Corrosion Engineers, Houston, TX.

[18] Moore, M. J. & Sieverding , C. H. (1976). "*Two-Phase Steam Flow in Turbines and Separators*", Chapter 6, Hemisphere Pub. Corp.

[19] Delp, G. A., Robison, J. D. & Dedlack, M. T. (1985). "*Erosion/Corrosion in Nuclear Plant Steam Piping: Causes and Inspection program Guidelines*", NP-3944, Electric Power Research Institute, Palo Alto, CA.

[20] Hirota, N. S. (1987). "*Erosion-Corrosion in Wet Steam Flow*", in *Metals Handbook.* 9th ed., *Vol.13 - Corrosion*, ASM International, Metals park, OH 964-971

[21] Chexal, B., Horowitz, J., Jones, R., Dooley, B., Wood, C., Bouchacourt, M. Remy, M. F., Nordmann, F. & St. Paul, P. (1996). "*Flow-Accelerated Corrosion in Power Plants*", TR-106611, Electric Power Research institute, PaloAlto, CA.

[22] Keller, H. (1974). VGB, *Kraftwerkstechnik*, *54*, No.5, 292.

[23] Izumia, M., Minato, A., Hataya, F., Ohsumi, K., Ohshima, Y. & Ueda, S. (1983). "*Corrosion and/or Erosion in BWR Plants and Their Countermeasures*", Water Chemistry and Corrosion Products in Nuclear Power Plants, International Atomic Energy Agency, Vienna, Austria, 61.

[24] Dooley, R. B. & Chexal, V. K. (2000). "Flow-accelerated corrosion of pressure vessels in fossil plants", *International Journal of Pressure Vessels and Piping*, *Volume 77*, Issues 2-3, February, 85-90.

[25] Fruzzetti, 1. K. (2004). "*Pressurized Water Reactor Secondary Water Chemistry Guidelines – Revision 6*", EPRI, Palo Alto, CA, 1008224.

[26] de. Bouvier, O. (1998). "*Influence of the Hydrazine Content on the Rate of Corrosion-Erosion of Carbon Steels – Report on Tests in the CIROCO Loop*", EDF-DER report dated December 8.

[27] de. Bouvier, O. (1999). "*Program on the CIROCO loop – Influence of Hydrazine on FAC in the presence of Oxygen – Program for Chrome*", presented at CHUG meeting, Portland, June 17-18.

[28] Cornell, R. M. & Schwertmann, U. (2006). "*The Iron Oxides"*, 2nd Ed., Wiley-VCH, 117.

[29] Verwey, E. J. W., Haaymann, E. L. & Romejin, F. C. (1947). *J. of Chem. Physics*, *15(4)*, 181.

[30] Ki-Sok Jung, & Laurent de Pierrefeu, (2010). *Corrosion Science*, *52*, 817–825.

[31] Didier Devilliers & Eric Mahe, (2007). "*Modified Titanium Electrodes*", in "*Trends in Electrochemistry Research*", Ed. By Magdalena Nunez, Nova Science Publishers, New York.

[32] Bard, A. J. & Faulkner, L. R. (2001). "*Electrochemical Methods"*, 2nd Ed., John Wiley & Sons, 751.

[33] Zhang, X. G. (2001). "*Electrochemistry of Silicon and its Oxides",* Plenum Publishers, 19.

[34] Freire, L., Novoa, X. R., Montemor, M. F., Carmezim, M. J. (2009). "*Materials Chemistry and Physics*", *114*, 962–972.

[35] Cornell, R. M. & Schwertmann, U. (2006). "*The Iron Oxides"*, 2nd Ed., Wiley-VCH, 235.

[36] Lyklema, J. (2010). *Current Opinion in Colloid & Interface Science*, *15*, 125-130.

[37] Bagotsky, V. S. (2006). "*Fundamentals of Electrochemistry",* 2nd ed., Wiley-Interscience, 275.

[38] Vijh, A. K. (1973). *"Electrochemistry of Metals and Semiconductors"*, Marcel Dekker, *45*.

[39] Lister, D. H. (1993). "*Activity transport and corrosion processes in PWRs"*, *Nuclear Energy*, *32(2)*, 103-114.

[40] Joshi, P. S. et al., (1993). *Corrosion*, *49(4)*, 300-309.

[41] Bignold, G. J., De Whalley, C. H., Garbett, K. & Woolsey, I. S. (1983). *Water Chemistry*, *3*, 219-226.

[42] Laurent de Pierrefeu, *"The Dissolution of Magnetite in High Temperature Water with the Influence of the Electrochemical Potential"* Draft for Master of Science and Engineering, University of New Brunswick, NB, Canada, 2009, 8.

[43] Allen, P. D., ampson, N. A H & Bignold, G. J. (1981). "*The Effect of the Potential on the Dissolution of Magnetite*", *Surface Technology*, *12*, 199-204.

[44] Bohnsack, G. (1987). "*The solubility of magnetite in water and in aqueous solutions of acid and alkali*", 161, Vulkan, Essen.

[45] Tremaine, P. R. & LeBlanc, J. C. (1980). *J. Solution Chemistry*, *Vo*. *9*, No. 6.

[46] "*Secondary Piping Rupture Accident at Mihama Power Station, Unit 3, of the Kansai Electric Power Co., Inc.*" (Final Report), Nuclear and Industrial Safety Agency, Japan, March 30, 2005.

[47] Sweeton, F. H. & Baes, J. R. C. F. (1970)., "The Solubility of Magnetite and Hydrolysis of Ferrous Ion in Aqueous Solutions at Elevated Temperatures", *Journal of Chemical Thermodynamics*, *Vol 2*, PT 4, 479-500.,

[48] Lister, D. H. & Lang, L. C. (2002). "*A Mechanistic Model for Predicting Flow-assisted and General Corrosion of Carbon Steel in Reactor Primary Coolants*", Proc. Chimie 2002, International water chemistry conf.

[49] Lister, D. H., Feicht, A., Cook, W., Khatibi, M., Liu, L., Ohira, T., Kadoi, E., Takiguchi, H., Fujiwara, K. & Uchida, S. (2007). *"Effects of Dissolved Oxygen on Flow-Accelerated Corrosion In Feedwater Systems",* International Conference on Environmental Degradation of Materials in Nuclear Power Systems, Whistler, BC, Canada, August.

[50] Khatibi, M., Lister, D. H., Feicht, A., Liu, L., Uchida, S., Fujiwara, K., Ohira, T., Takiguchi, H. & Hisanume, K. (2009). *"Parameters influencing flow-accelerated corrosion (FAC) in the secondary side of nuclear power plants"*, Submitted for the 30th Annual Conference of the Canadian Nuclear Society, Calgary, Alberta, Canada, May 31 - June3.

[51] Keith Fruzzetti and Christopher J. Wood, (2006). "*Developments in Nuclear Power Plant Water Chemistry*", International Conference on Water Chemistry of Nuclear Reactor Systems, 2006 Jeju Island, *The Republic of Korea*, October 23–26.